TRI-SERVICE 2007 CORROSION CONFERENCE
ARMY • NAVY • AIR FORCE • MARINES • COAST GUARD • NASA

Surface Pretreatment Based On Dilute Hexafluorozirconic Acid

Y. Zhai*, Z. Zhao*, G.S. Frankel*, J. Zimmerman**, T. Bryden** and W. Fristad**
*Fontana Corrosion Center
The Ohio State University
Columbus, OH 43209
**Henkel Corp.
Madison Heights, MI 48071

ABSTRACT

Two surface pretreatments based on dilute hexafluorozirconic acid (FZ) solution, a simple FZ and a modified FZ or MFZ, were studied as replacements for the phosphating process. The FZ conversion coatings were deposited on cold rolled steel (CRS) substrates by immersion treatment. AFM images reveal that the coating surface exhibited small features tens of nm in size and clusters of these features that are on the scale of microns. The MFZ coating contained more and larger clusters than the coating formed in the simple FZ bath. Such features were invisible in SEM images where the surfaces looked quite smooth. The polarization resistance of CRS in sodium chloride solution was slightly increased by FZ treatment, and a little more by MFZ. Electrochemical impedance spectroscopy (EIS) tests showed that MFZ-treated CRS covered with paint provided better long-term corrosion protection performance than the FZ/paint system during immersion in chloride solution. The performance of the system with MFZ was comparable to that of phosphate conversion coatings. TEM images showed that the MFZ coating is about 20 nm thick, continuous and adherent to the substrate. Major components are Zr, Fe and O. The MFZ pretreatment is environment-friendly as the treatment solution is phosphate-free and dilute.

Keywords: surface pretreatment, phosphate conversion coating, corrosion protection performance, cold rolled steel

INTRODUCTION

Organic coatings have been widely used for corrosion protection of metals in the manufacturing and construction industries. Surface pretreatment of the substrate metals is usually required before paint application to promote paint adhesion and improve corrosion performance. The most common surface pretreatment for both ferrous and non-ferrous metals is phosphating, which results in a reasonably hard, electrically non-conducting surface coating of insoluble phosphate that is contiguous and highly adherent to the underlying metal [1,2]. Phosphating plays a vital part in the automobile, appliance and general manufacturing industries. However, the phosphating process has several limitations:

1. Concentrated phosphate bath is used [1] and phosphate has detrimental impact on ground and surface water ecology and the sustainability of water resources. Although costly waste treatment and disposal are in use, phosphate-free environmental-friendly solutions are desired.
2. Significant sludge generation in the concentrated phosphate bath necessitates frequent desludging [2].
3. Phosphate conversion coating usually is porous and requires an additional sealing procedure [2].
4. Typically phosphating is carried out at a raised temperature [2], requiring expensive energy.

Research on new surface pretreatments to replace phosphating and phosphate conversion coatings has been performed. One promising new pretreatment is the application of zirconium oxide (ZrO_2) on metal surface by the sol-gel method [3-7] or by immersion in or rinse with hexafluorozirconic acid (H_2ZrF_6) solution [8-13].

Homogeneous, non-cracked zirconia coatings on mild steel were obtained by the sol-gel method and found to be corrosion protective according to the results of potentiodynamic polarization tests [6]. Maggio and coworkers studied the formation of ZrO_2 coatings on low-carbon steel [4, 5] and aluminum sheet [7] with various organic or inorganic precursors and compared the adhesion and corrosion protection of the coatings with commercial phosphate and chromate conversion coatings. Using an optimized sol-gel process the resulting zirconia coatings were thin (about 20~400 nm) and amorphous. The authors concluded that sol-gel zirconia coatings could provide similar or even better corrosion protection performance compared with the phosphate coatings by promoting adhesion although the new coating did not act as a barrier [7].

Puomi et al. investigated a commercial hexafluorozirconic acid (FZ) based pretreatment on galvanized steel [8-10]. The treatment time was 2-60 s at temperature of 20-40°C and the bath concentration varied from 1.6-4.8 g/l FZ (700~2100 mg/l Zr) with a pH value of 3.6-4.0. The thickness of the zirconium coating was about 50 nm on hot-dipped galvanized steel and slightly thinner on galvanized steel coated with a ZnAl layer. Prohesion test results show that zirconic acid rinse pretreatment provided similar corrosion performance to zinc phosphate and chromic acid rinse treatment [8]. X-ray photoelectron spectroscopy (XPS) results suggested that the zirconium on the surface was mainly in the form of ZrO_2. Fluorine was also observed as a result of adsorbed ZnF_2 and unreacted physically adsorbed FZ [9], which can be removed by water rinse after the pretreatment [8].

Recently, non-commercial zirconium and titanium fluoride-based coatings were studied on a magnesium alloy substrate (AM60) by Verdier et al [11, 12]. The H_2ZrF_6 concentration was varied from 10^{-3} to 10^{-1} M (90~9000 mg/l Zr).). The film formation was believed to proceed by precipitation of the Zr and Ti complexes initiated by the increase of interfacial pH related to the reduction of water [11]. It was found that low FZ concentration (10^{-3} M) favors the formation of ZrO_2 because the precipitation of the metal cation is through the oxolation[1] reaction only. In the more concentrated FZ solutions (10^{-1} M) several zirconium compounds will form by both olation[2] and oxolation reactions. The effects of pH and fluoride ions were also discussed [12]. For $5x10^{-1}$ M H_2ZrF_6, the increase of pH from the original 2.2 to 5.3 improved the coating performance. Less zirconium was deposited on the surface with fluoride addition because it makes the solutions more aggressive with respect to the AM60 alloy.

In this paper, two surface pretreatments based on dilute hexafluorozirconic acid (FZ) solution, a simple FZ and a modified FZ or MFZ, were studied as replacements for the phosphating process. The concentration of FZ is less than 100 mg Zr/l for the simple FZ treatment. In MFZ, the same low amount of FZ is used and in addition, other non-hazardous ingredients and present in small amount are included. The two FZ coatings were characterized with atomic force microscopy, scanning electron microscopy

[1] Oxolation is a reaction of condensation between two coordinate metal complexes by a hydroxo (HO) ligand: M-OH+M-OH → M-HO-MOH → M-O-M +H_2O [11].

[2] Olation is a reaction of condensation between two coordinate metal complexes by an aquo (H_2O) ligand: M-OH +M-OH_2 → M-HO-M+H_2O [11].

and energy dispersive spectroscopy; their electrochemical activities with and without primer paints were evaluated and compared.

The coating structure and composition of MFZ, the superior one among the two FZ coatings, was further studied with transmission electron microscope. The comparison of the corrosion protection of MFZ and commercial phosphate treatments was made with electrochemical impedance spectroscopy monitoring during two-month stagnant immersion of the fully painted cold rolled steel samples in sodium chloride solution. The MFZ pretreatment is environment-friendly as the treatment solution is phosphate-free and dilute. Furthermore, the treatment involves simple immersion at nearly room temperature conditions and there is no need of chromic acid sealing after the treatment.

EXPERIMENTAL

Materials and sample preparation: Cold rolled steel (CRS, ACT Laboratories, Hillsdale, MI) was used as the substrate for this study. As-received CRS samples were cleaned with an alkaline cleaner (8% Parco® Cleaner1200, Henkel Corporation, Surface Technologies, Madison Heights, MI) and then washed with warm DI water before the treatment. In the surface microscopic characterizations, polished CRS samples were used as model substrates to avoid the complications from large (up to tens of microns) features present on as-received CRS surfaces. Samples with size about 1cm x 1cm were abraded with SiC paper to 1200 grit and then polished with 1 μm diamond paste (Buehler) in ethyl alcohol. Polished samples then were cleaned in an ultrasonic ethyl alcohol bath. Surface pretreatment was carried out soon after the polishing.

Surface pretreatment of CRS: Two immersion treatments were compared: (1) dilute (Zr < 100 mg/l) FZ bath. The FZ bath was prepared by mixing 20 wt% of FZ (Advance Research Chemicals Inc., Catoosa, OK) with DI water. (2) MFZ bath (commercially available as Bonderite® NT-1, Henkel Corporation, Surface Technologies, Madison Heights, MI) contained the same amount of FZ as in the FZ bath. Both solutions were adjusted to pH=4.5~5 with Parco® Neutralizer 700 (5~15% of ammonium bicarbonate, Henkel Corporation, Surface Technologies, Madison Heights, MI). The immersion treatment consisted of the following steps:

1. Rinse samples with cold deionized (DI) water
2. FZ or MFZ immersion treatment: 30~35°C, pH = 4.5-5.0, 60s
3. Rinse treated samples with cold DI water
4. Air dry treated samples and store in a desiccator.

Preparation of painted CRS panels: CRS samples were given different pretreatments and then painted. Four paints were used in this study: Vectrogard® 900 (Valspar, Moline, IL), CathoGuard® 310B (BASF Corporation, Southfield, MI), Corvel® Sunburst 40-2016 (Rohm and Haas, Philadelphia, PA), and Duracron® 100 (PPG industrial Inc., Pittsburgh, PA). The Vectrogard and Cathoguard paints were applied by electrocoating (e-coat) process in which paint is electrodeposited onto the metal substrates. The average film thickness of Cathoguard was 0.9 mil after baking for 20 minutes at 350°F. Corvel, a powder coating, was applied electrostatically to a film thickness of about 1.9 mil after curing at 400°F for 7 min. Duracron is a solvent-borne spray coating; the film thickness was about 1.3 mil after baking for 10 min at 400°F.

Open circuit potential (OCP) and polarization resistance (R_p) tests: The trends of OCP (corrosion potential) and Rp of polished CRS samples with and without FZ coatings were monitored for 30 min in 0.1 mol/l Na_2SO_4. A three-electrode flat cell was used for the tests. Reference and counter electrode were saturated calomel electrode (SCE) and platinum (Pt) mesh, respectively. A Gamry PC4 potentiostat (Gamry Instruments, Warminster, PA) was used.

Stagnant Immersion and Electrochemical Impedance Spectroscopy (EIS) Tests: Corrosion protection performance of fully painted CRS samples with different conversion coatings and paints was

evaluated under stagnant immersion conditions. Plastic cylinders with inner diameter of 4 cm or 6 cm were glued onto the painted sample surfaces. About 50 (for 4 cm cylinder) or 75 ml (6 cm cylinder) 0.5 mol/L NaCl solution was poured into the cylinders. EIS tests were run periodically with either a PAR 263 potentiostat (AMETEK Princeton Applied Research, Oak Ridge, TN) and SI 1255 HF frequency response analyzer (Solarton Instruments, Houston, TX) or a Gamry Reference 600 potentiostat (Gamry Instruments, Warminster, PA). The SCE reference electrode and the carbon rod counter electrode were placed into the tube for each measurement. The frequency range was 100 kHz to 10^{-2} or 10^{-3} Hz. The perturbation amplitude was 10 mV around the OCP. Fitting and simulation of the impedance data was done with Zview2.90 software by Scribner Associates Inc.

Atomic Force Microscopy (AFM): Mapping of topography and Volta potential was performed in air before and after pretreatment using a Dimension 3100 AFM (Digital Instruments Veeco, Santa Barbara, CA). Pt/Ir coated probes with a resonance frequency of 40-70 KHz (Model SCM-PIT, Veeco Probes, Santa Barbara, CA) were utilized in both contact and tapping mode AFM. In contact mode, the setpoint potential (SP) was 0.2~0.5 V; in tapping mode AFM, SP=1.0V. Scan rate was 0.5 ~ 1 lines/s and the scanned area contained 512 x 512 points.

Scanning Electron Microscopy (SEM) and Energy Dispersive Spectroscopy (EDS): FZ coated CRS samples were examined with an SEM (Philips XL30 ESEM FEG) using an acceleration voltage of 15 keV. Combined with EDS analysis (Genesis Spectrum, EDAX, AMETEK, Inc.) and backscattered electron imaging (BEI), chemical compositional information on the surface was obtained.

Focused Ion Beam (FIB) and Transmission Electron Microscopy (TEM): High-resolution TEM was performed to study the compositional and structural features in the MFZ coating on CRS. The TEM specimen was prepared using a FIB tool (FEI Strata DB235) at 30 keV with a Ga+ ion source. Before the ion milling, a 1μm-thick Pt layer was deposited onto the surface to protect the thin conversion coating. The FIB preparation consisted of two steps. First, a relatively large sample with size about 25 μm x 6 μm x 4 μm was milled from the bulk sample in the FIB chamber. Two trenches were milled on either side of the site of interest and the area in the middle was thinned to 4μm. In the second step, this large sample was "welded" to the surface of a Cu support grid using the platinum deposition inside the FIB and then the specimen was further low-energy ion milled until achieving a thickness of about 50~120 nm. This approach was required to hold the CRS substrate in place in the presence of the magnetic field of the TEM.

Scanning TEM (STEM) was used for Z-contrast imaging to obtain compositional and structural information of the very thin conversion coatings. Z-contrast images are formed by collecting high-angle (75-150 mrad) elastically-scattered electrons with a high angle annular dark-field (HAADF) detector. Some of the dark field images were inverted, making pseudo bright field images. All TEM studies were carried out with a Tecnai TF-20 TEM.

RESULTS AND DISCUSSION

FZ vs. MFZ pretreatment

The two FZ treatments were compared in terms of surface morphology, composition and electrochemical activities.

Topography: Topographic images from an atomic force microscopy were obtained for polished CRS samples before and after the FZ treatment. Figure 1a and b show a 1μm x 1μm square of an as-polished CRS surface before the FZ treatment. With 1 μm –diamond paste polishing finish, some submicron scratches were left on the surface and there small 'debris' particles were observed around the scratches. The surface morphology for the two samples that were used later for FZ and MFZ treatment looked very similar to each other. The polished CRS sample was immersed in the FZ or MFZ bath at

30°C for 60 s. Figures 1c and d are AFM images of MFZ treated CRS. Nodules on the scale of tens of nm in size and clusters of these nodules hundreds of nm in size are observed on the surface. It seems that these features densely covered the substrate surface because no features from the original (as-polished) substrate surface can be seen in these high resolution images after the treatment. The surface with simple FZ treatment appeared similar to the MFZ coating as shown in Figure 1e and f. However, the nodules on the FZ treated surface appeared to be finer in size and formed fewer clusters than those on the MFZ coating.

The treatment was also carried out at a higher treatment temperature of 35°C for the same amount of immersion time 60 s. The AFM images of the treated CRS samples are shown in Figure 2. Again, a nanostructured coating was obtained on the surface after the 35°C FZ and MFZ treatment. Figures 2b and c are 1µm x 1µm images of the MFZ coating. Larger clusters are seen on the surface than the clusters formed at the lower temperature of 30°C. The coating surface became quite rough as a result of the formation of large clusters (Figure 2a, the 10µm x 10µm image of MFZ). On the FZ coating bigger nodules were also formed at 35°C (Figure 2e and f) compared with those at 30°C (Figure 1e and f). Nevertheless, much fewer clusters of the nodules can be seen on FZ than on MFZ at this higher temperature. The FZ coating obtained at 35°C thus was smoother than the MFZ as the topography image of a larger window size (Figure2d, 10µm x 10µm image) reveals.

SEM/EDS surface morphology and compositions: The FZ and MFZ coatings were examined by SEM and EDS analyses were performed to obtain the compositional information of the coatings. The secondary electron (SE) and back-scattered electron (BSE) micrographs of polished CRS after MFZ (top row) and FZ (bottom row) treatment are shown in Figure 3. In the SE images, Figures 3a and d, the surface after the treatment was almost as smooth as the as-polished surface with scratches from the polishing procedure clearly seen. No fine structures can be seen with the SEM; the fine detail revealed by AFM is not visible in the SEM micrographs. Small dark spots looking like pits are seen on the coating surface as shown in the topography BSE images in Figures 3b and e. Some were present before the treatment as a result of polishing in DI water and others were produced during the immersion treatment. The BSE images in Figure 3c and f mainly reflect the contrast in Z number. The uniform look of the compositional BSE images suggests that both the FZ coatings fully covered the substrate surface. The pits were dark which indicates that they contain lighter elements. The two FZ coatings look similar under SEM except that smaller pits were found on the simple FZ coating, which might be related to slight differences in the polishing of the substrates.

EDS of the smooth surface of the MFZ and FZ coating and on a typical pit in the MFZ coating are presented in Figure 4. EDS is not an extremely surface sensitive technique, but the major elements observed in the FZ coating surface are iron (Fe), oxygen (O), Zr and carbon (C). In addition, some aluminum (Al) and silicon (Si) were detected with a very small peak. The quantifications of the EDS are listed in Table 1. A large amount of Fe was detected most of which was probably from the substrate because the coating is very thin (around 20nm, as will be reported below). The typical (smooth region) MFZ coating contains about 0.76wt% of Zr, 1.33% of O and 1.08% of C. The coating might contain some fluorine but its relative concentration is unknown due to interference with Fe. Some manganese was also detected which most probably was from the substrate inclusions. The composition of the FZ coating was similar to the MFZ except that higher amount of Zr and Al were found in the FZ coating. More light elements such as O, C and Si were present in the pit. Furthermore, high Zr was detected in the pit, which indicates pits were also well covered with the main coating elements.

Electrochemical studies: Electrochemical reactivity of the FZ coatings was investigated both with unpainted CRS and with a fully painted system. The OCP and linear polarization resistance (Rp) were measured as a function of time for FZ treated CRS samples in a mildly aggressive solution of 0.1 mol/L Na2SO4. Polished CRS substrates were used and treatment time was 60s at 30°C. Figure 5a shows the time series of OCP for non-coated (line without symbols), MFZ-coated (solid circles), and FZ-coated

(open squares) CRS. The OCP of the as-polished CRS continued to decrease as the exposure time increased. The coverage of the FZ coatings reduced the initial OCP by about 220mV and slowed down the decrease of OCP with time. In fact, as exposure time increased the OCP of coated CRS started to increase and got close to that of the bare polished CRS. The effect of coating on OCP almost diminished after about 30 min immersion in the sulfate electrolyte. The OCP of the MFZ coating was slightly lower than that of the FZ coating during the 30 min test in sodium sulfate solution.

Figure 5b shows that the R_p of bare CRS underwent an increase within the first 300 s immersion to about 1500Ω (with testing area of 0.785 cm^2). It then remained almost constant with some fluctuations throughout the rest of the test time. Both MFZ and FZ treatment improved the corrosion resistance of CRS at the beginning of the exposure test. The R_p of treated CRS increased first with time and then started to decrease after about 300 s exposure. The maximum R_p at 300s for MFZ treated sample was about 9000 Ω, which is nearly twice of the maximum R_p for the FZ treated sample and fours time of that of the bare CRS. However, by the end of the testing (30 min) R_p of both MFZ and FZ treated samples had decreased to a low value comparable to that of the uncoated sample. Note that polarization resistance scales inversely with corrosion rate. Therefore the results of the OCP/ R_p tests show that some weak protection is provided by the FZ coatings but it only lasts for a short time. The MFZ coating exhibits higher average R_p than the FZ coating. The combined decrease in corrosion rate and corrosion potential from the FZ or MFZ treatment suggest a decrease in the kinetics of the cathodic reaction, which is likely dominated by oxygen reduction in this stagnant, air exposed, and neutral electrolyte.

To better compare the performance of the two pretreatments, MFZ- and FZ-treated CRS samples were painted with an electrodeposited primer, Valspar Vectrogard® 900, and immersed in 0.5 mol/L NaCl for about two months. EIS tests were performed periodically to monitor the change of the impedance of each system as a function of immersion time. All EIS measurements reported in this section were made with the PAR 263A system.

The EIS spectra from the first three days of immersion are shown in Figure 6a. The absence of typical semicircles in the Nyquist plot of the MFZ impedance data indicates the absence of electrochemical reactions and show that the paint system was very protective. The low frequency impedance can be considered to be the sum of the pore resistance, R_{po}, assuming a defective coating, the charge transfer reaction resistance at the base of pores, R_{ct}, and the solution resistance, R_s. After 6 h immersion, the impedance magnitude (|Z|) at the lowest testing frequency of 0.01Hz was higher than 10^{10} Ω.cm^2. This high impedance value is further evidence that the substrate was well protected by the MFZ/paint coating system. Figure 6a also shows that the impedance spectra of the MFZ sample exhibited little change and retained a high impedance during the first 3 days of immersion.

After 6 h immersion, the FZ sample exhibited a small semicircle (solid line without symbols in Figure 6a) and a very low impedance, indicating a worse corrosion protection than the MFZ sample. However, the impedance of the FZ sample increased during the first 24 hrs immersion and reached about same value of the MFZ sample at the third day.

The impedance data at longer immersion time for both samples are presented in Figure 6b. The low frequency impedance values of the two samples were similar from about 3-24 days, though the MFZ sample impedance was always somewhat higher. The low impedance value for the FZ sample at 6 days seems to be erroneous data. After 24 days the FZ sample started to degrade and its low frequency impedance became about 10x lower than that of the MFZ sample.

A defective coating system can be modeled with an equivalent circuit that contains two time constants as shown in Figure 7 [14]**.** The resistances have been explained earlier. Two constant phase elements (CPE) are also included in this model: CPE_c is the coating capacitance and CPE_{dl} represents the capacitance of the double layer at the pore bottoms.

The equivalent circuit component values obtained by fitting of the EIS data for MFZ and FZ samples are presented in Figure 8. For both samples during the 57 days immersion, R_{ct} values were about 100 times larger than R_{po} values (Figure 8a). Both R_{ct} and R_{po} of the MFZ sample (solid curves)

did not change much with immersion time. However, the R_{ct} of the FZ sample started to decrease while its R_{po} increased at times greater than 20 days (dashed curves). This might be an indication of a reaction under the coatings creating corrosion products that filled up the pores in the primer (an increase of R_{po}).

The evolution of the CPE magnitude in Figure 8b indicates that the coating capacitance of both samples was almost constant during 57 days immersion and that of the MFZ sample was slightly smaller than that of FZ. The double layer capacitance of the MFZ sample was lower than that of the FZ sample and almost constant during the test. The CPE exponents for the coating of both samples and for the MFZ double layer were close to 1 during the tests, which implies these components behaved similarly to a perfect capacitor. The double layer of the FZ sample was an exception with CPE-α <1 (dashed line with open diamonds) and the CPE magnitude (dashed line with open circles) always increased with time.

To summarize, the EIS results show that MFZ pretreatment combined with a primer provide good corrosion protection to CRS. The FZ pretreatment exhibited an impedance that initially was high, but then degraded with time.

MFZ coating structure

The MFZ coating was further studied because of its superior corrosion protection performance compared to the FZ when combined with a primer. TEM and EDS analyses of a MFZ coating on non-polished CRS were performed to study the coating structure and composition. A TEM HAADF (high angle annular dark-field) image of a FIB (focused ion beam) prepared specimen with thickness about 120nm is shown in Figure 9a. Gold (Au) and Pt protective layers were deposited on top of the coating before the FIB milling. Because this image is pseudo-bright field, the high-Z Au and Pt layers look dark. The coating is brighter than the substrate, CRS, which indicates the coating had a lower density or lower average Z number. This probably results mainly from oxygen in the layer. The coating thickness was around 20 nm, but it varied somewhat along the substrate surface. The variation in transmitted electron intensity indicates that the oxide in the coating was not uniform. Some dark round particles (such as Site A in Figure 9a) with size up to 10 nm are seen in the coating; the darkness of the particles indicates higher Z number or density.

With a thinner sample thickness of 60 nm, higher magnification TEM images of MFZ coated CRS can be obtained. In Figure 9b the TEM image shows detailed structure of the MFZ coating on a recessed region of the substrate. The coating is adherent to the steel substrate. At this particular region, the coating density near the substrate is lower than that at the outer surface as indicated by the lighter color in the pseudo-bright field image. Also, clusters of very small dark particles are formed in the outer half part of the coating. The darkness in this image suggests higher Z number.

Spot EDS was performed at selected sites in the MFZ coating. Figure 10a shows the spectrum obtained at Site B in Figure 9b, an outer part of the coating with relatively higher density (darker color). C, O, Fe, Si, Zr, Au and Cu were detected. The large C signal may come from contamination inside the TEM. Cu probably comes from the grid where the specimen was attached. The treating solution and the substrate do not contain Au; Au should come from the adjacent Au protective layer during FIB ion-beam milling. Unfortunately, in the EDS the Zr-L and Au-M peaks, the strongest signals for Au and Zr, are almost fully overlapped at around 2 keV. However, the weaker peaks of ZrK (around 15 keV) and AuL (around 10 keV) are distinct. The MFZ coating at this spot thus mainly consists of Fe, Zr, and O. At a site closer to the substrate (Site C in Figure 9b), approximately 3x more Fe and O were detected in the coating as shown in Figure 10b. The Zr peak is also higher than that at Site B. It should be the higher amount of the lighter elements such as Fe and O in the coating that contributes to the brighter color close to the substrate.

MFZ vs. phosphate pretreatment

EIS studies were also conducted to compare the corrosion protection behavior of MFZ coating with zinc and iron phosphate conversion coatings and then with different paints. A sample matrix was

tested consisting of samples with three conversion coatings and three primers. The three paints were Cathoguard (labeled as e-coat), Sunburst (powder), and Duracron (solvent-borne). All samples were immersed continuously in 0.5 mol/L NaCl for about two months. Two batches of tests with duplicate samples were performed for reproducibility. The EIS results in this section are mainly from the first batch of the tests (lasted for 70 days) except for the solvent-borne painted sample with MFZ coating which was taken from the second batch (60 days) because the duplicate sample in the first batch was an outlier and failed at an unusually early time of the test, probably as a result of a coating defect. The other duplicate samples from the two batches of tests exhibited similar behavior.

The initial EIS measurements were performed with a PAR 263A system. The Gamry Reference 600 system was used for all measurements after the 24th day of the first batch tests and 11^{th} day of the second batch tests (Solvent-borne/MFZ sample). The Gamry system provided higher quality data with less noise in the low frequency region. As a result, the lowest frequency tested was decreased toward the end of the tests from 10^{-2} Hz to 10^{-3} Hz. This provided a more accurate assessment of the low frequency impedance and allowed better differentiation of sample behavior.

The EIS spectra at or close to the end of the immersion tests (at the 60^{th} day for the solvent-borne paint samples and at the 70^{th} day for e-coat and powder paint samples) are shown in Figure 11. With powder paint (medium line width) all the three impedance curves of the samples with the various pretreatments were capacitive with a nearly constant 90 degree phase shift in the phase Bode plot (Figure 11b), indicating that protection was achieved for all three pretreatments with the powder paint. Zn phosphate coating (dashed lines) was the best of the three conversion coatings and its impedance at 1 mHz, $|Z|_{0.001HZ}$, after 70 d was around $3x10^{11}$ Ω-cm^2. The sample with MFZ coating (solid lines) was only slightly worse than that with the Zn phosphate coating and better than the Fe phosphate coating (dotted lines).

The EIS spectra for samples with solvent-borne paint are plotted with the thinnest lines in Figure 11. The sample with Fe phosphate coating still had high impedance values ($|Z|_{0.001Hz}$~$1x10^{11}$ Ω.cm^2) at the 60^{th} day of immersion. The MFZ coating performed as well as the Fe phosphate coating. In contrast, the Zn phosphate coating degraded faster than the other two (dashed thinnest line in Figure 11b).

From Figure 11 it appears that e-coat paint (boldest lines) is the worst of the three paints because the impedance values were the lowest observed at the end of the immersion tests for all three conversion coatings. Nevertheless, the final impedance magnitudes were still as high as 10^{10} Ω.cm^2 and it can be concluded that, with e-coat paint, MFZ coating is almost equally protective as the phosphate coatings by the end of 70 days exposure.

The EIS monitoring of all the samples during the two-month stagnant immersion is summarized in Figure 12 where $|Z|_{0.001Hz}$ is plotted vs. exposure time. Because of the lack of data at frequency 0.001 Hz in the spectra acquired at the earlier times, EIS data fitting using the model shown in Figure 7 was performed for these samples and the impedance was extrapolated to 0.001 Hz. Note that the data from the early exposure times are noisy and possibly inaccurate because of the use of the less accurate equipment.

It is obvious that among the three paints, the powder paint (curves with medium line width) exhibited the highest impedance and therefore the best corrosion protection performance. The solvent-borne paint (thinnest lines) was better than the e-coat (boldest lines) at shorter exposure times, but exhibited poor long term performance with phosphate conversion coating. MFZ provides similar protection behavior as Zn and Fe phosphate coating for the powder and e-coat paints. For the solvent-borne paint, MFZ seems to be the best conversion coating.

CONCLUSIONS

Surface pretreatments in dilute hexafluorozirconic acid (FZ) solution and a modified FZ treatment (MFZ) were evaluated as replacements for the phosphating process before primer paint application. The following was observed:

- AFM studies of FZ coatings on CRS revealed that the coating surface exhibited small nodules tens of nm in size and clusters of these features that were on the scale of hundreds of nanometers to microns. Finer individual nodules and fewer clusters were formed in the FZ treatment than in the MFZ treatment.
- Both FZ and MFZ coatings look smooth under SEM examination because the fine features revealed by AFM are invisible in SEM. Fe, Zr, Si, and O were detected on the coating surface with EDS. Coating also formed on pits.
- Some weak protection was provided by the FZ and MFZ coating for CRS in a mildly aggressive neutral sulfate environment but it only lasted for a short time. More improvement in the corrosion resistance is achieved by MFZ.
- With paint, FZ treated CRS sample exhibited initially high impedance, but it degraded fast with time. In contrast, long-term good performance can be achieved with the MFZ treatment.
- Results of electrochemical tests on painted CRS samples with different conversion coatings show that the MFZ treatment combined with electrodeposited, powder or solvent-borne paints provided corrosion protection performance comparable to phosphate conversion coatings.
- Z-contrast TEM images showed that the MFZ coating was about 20 nm thick, continuous and adherent to the substrate. The major components are Zr, Fe and O; More Fe and O are in the coating near the substrate.

Table 1: Quantification of the spot EDS in Figure 4.

Wt%	**OK**	**CK**	**SiK**	**FK**	**AlK**	**ZrK**	**MnK**	**FeK**
MFZ	1.33	1.08	-	1.18	0.04	0.76	0.37	95.24
FZ	1.53	1.44	-	0.92	0.36	1.49	-	94.27
Pit-MFZ	2.7	3.02	0.62	0.76	0.1	3.4	0.41	88.99

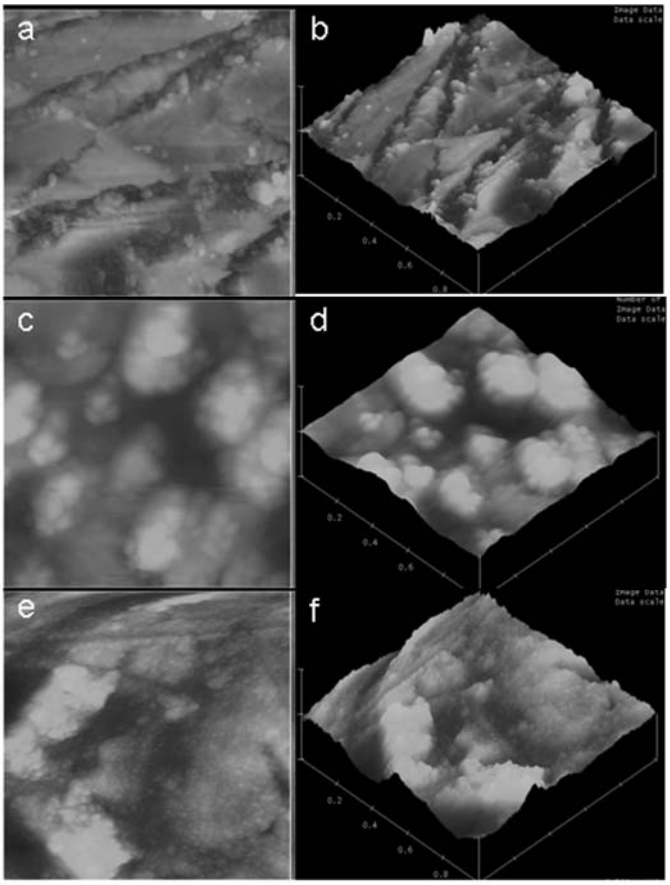

Figure 1: AFM topography of FZ immersion treated CRS. Treatment conditions: 30°C for 60s. Imaging window size= 1μm X 1μm, z range=50nm. (a-b) Before treatment, 1μm-finish as polished. (c-d) After MFZ treatment. (e-f) After FZ treatment.

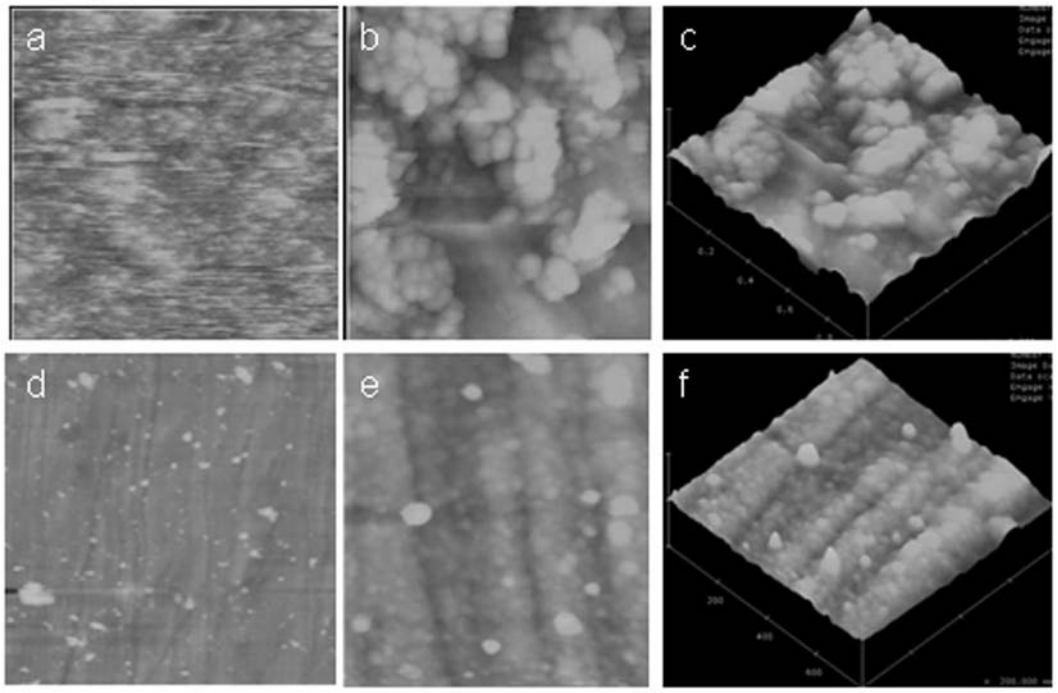

Figure 2: AFM topography of FZ immersion treated CRS. Treatment conditions: 35°C for 60s. Left column: imaging window size= 10μm X 10μm, z range=250nm. Middle and right columns: window size=1μm X 1μm, z range=50nm. (a-c) After MFZ treatment. (d-f) After FZ treatment.

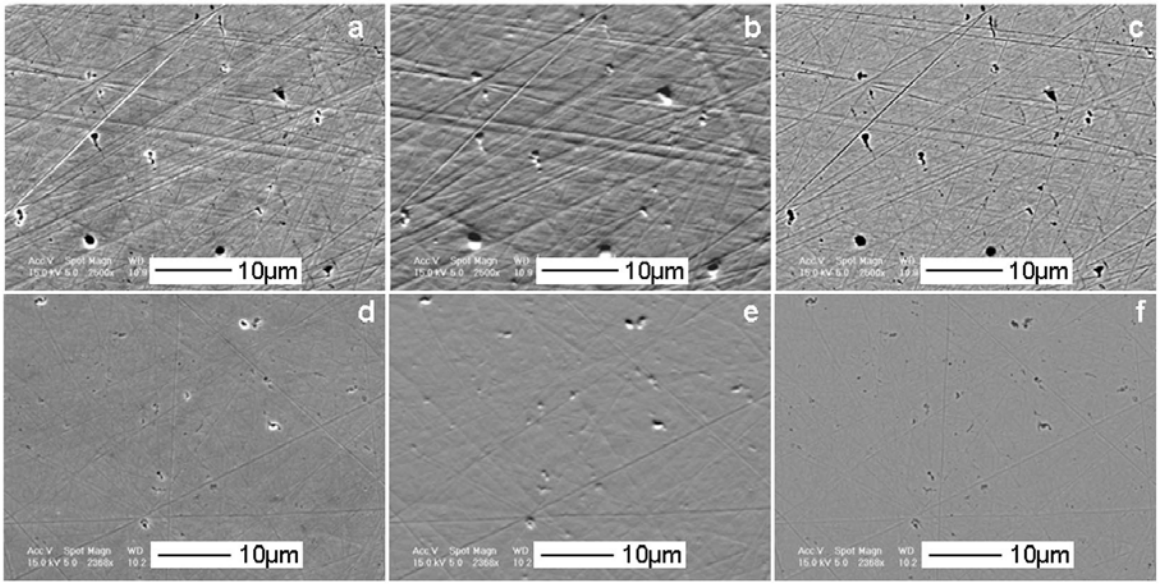

Figure 3: SEM micrographs of FZ immersion treated CRS. Left column: Secondary electron images. Middle column: BSE topography images. Right column: BSE compositional images. (a-c) MFZ treated samples. (d-f) FZ treated samples.

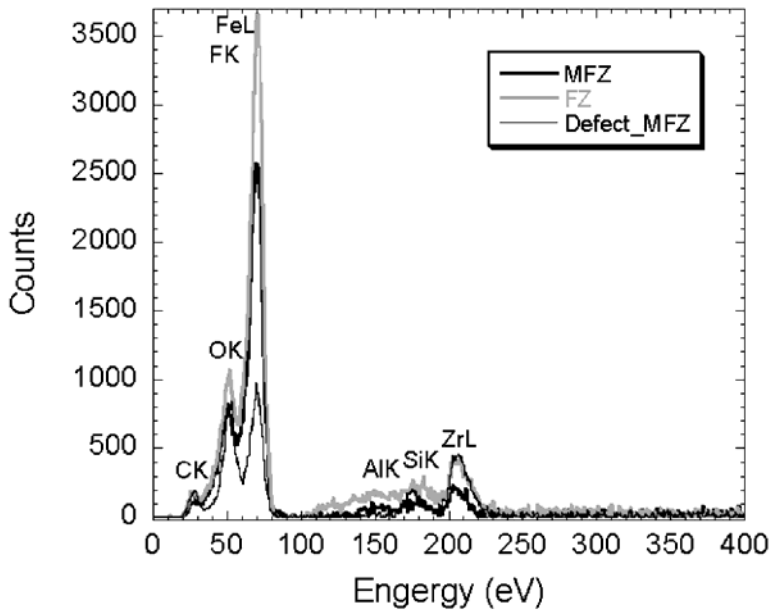

Figure 4: Spot EDS on the FZ and MFZ coatings. Beam voltage = 15kV, Spot = 5, collection area about 2μm X 2μm.

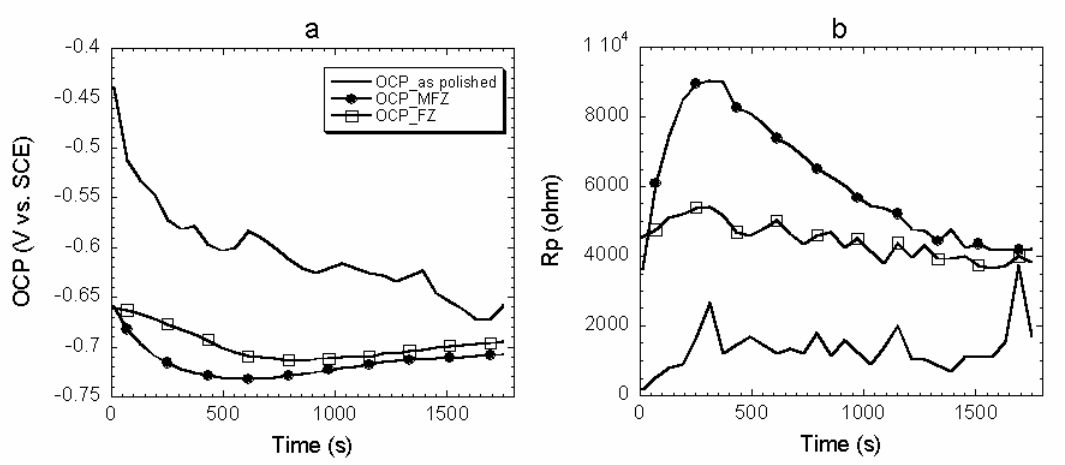

Figure 5: OCP (a) and polarization resistance (b) trends of CRS in 0.1M Na_2SO_4.

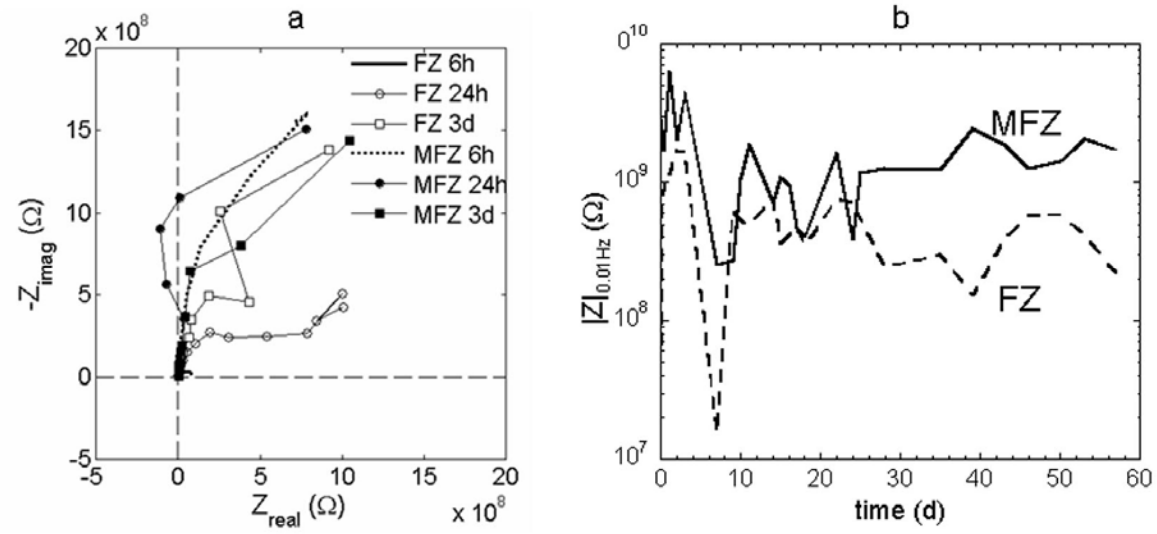

Figure 6: Electrochemical impedance spectra of fully painted CRS panels with FZ conversion coatings in 0.1mol/L Na_2SO_4. Testing area was 14.6 cm^2. (a) Nyquist plots of the first three days EIS data for both FZ and MFZ. (b) Trends of impedance magnitude |Z| at 0.01Hz for FZ (dashed curve) and MFZ (solid curve) coated CRS.

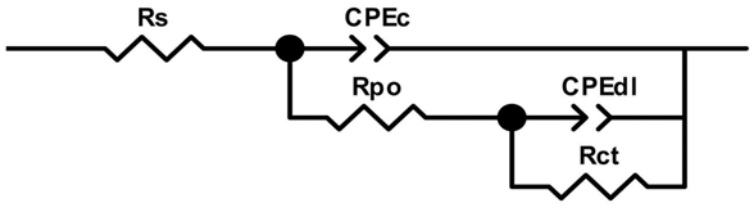

Figure 7: Equivalent circuit for the painted system.

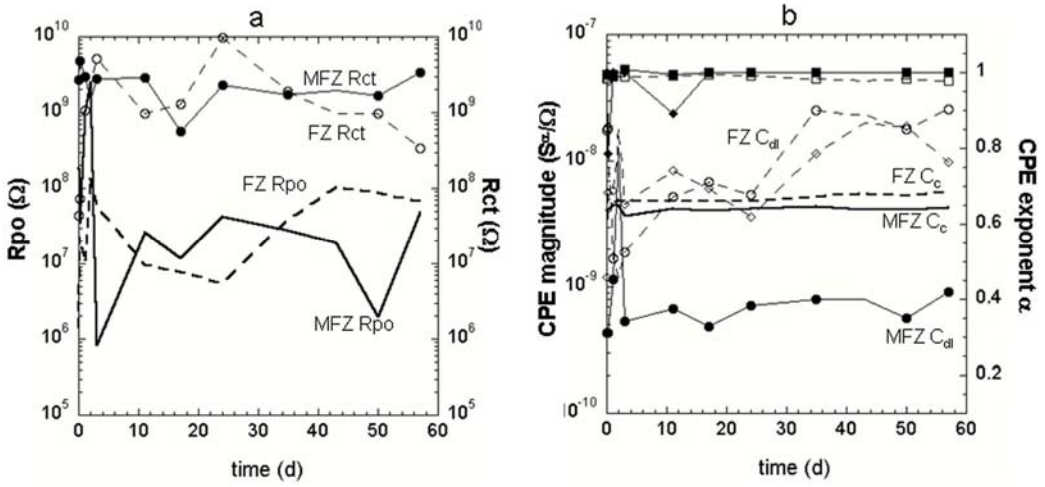

Figure 8: Fitted resistance (a) and capacitance (b) of FZ and MFZ coated CRS. For CPE exponent curves in (b): solid squares-MFZ CPEC; solid diamonds-MFZ CPEdl; open squares-FZ CPEC; open diamonds-FZ CPEdl.

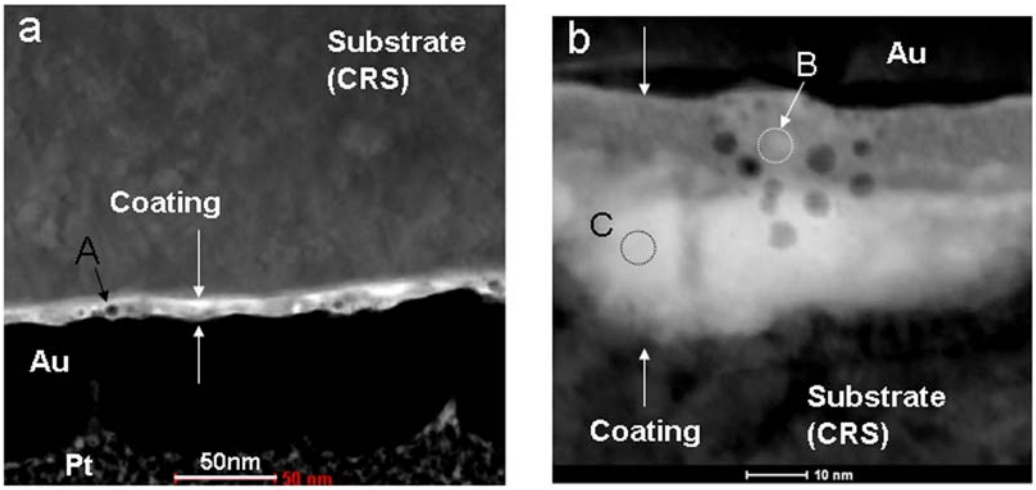

Figure 9: STEM HAADF images of MFZ pretreated CRS. Images were converted to pseudo-bright field. (a) Lower resolution image obtained with a specimen thickness of 120nm. (b) Higher resolution image obtained with thickness of 60nm.

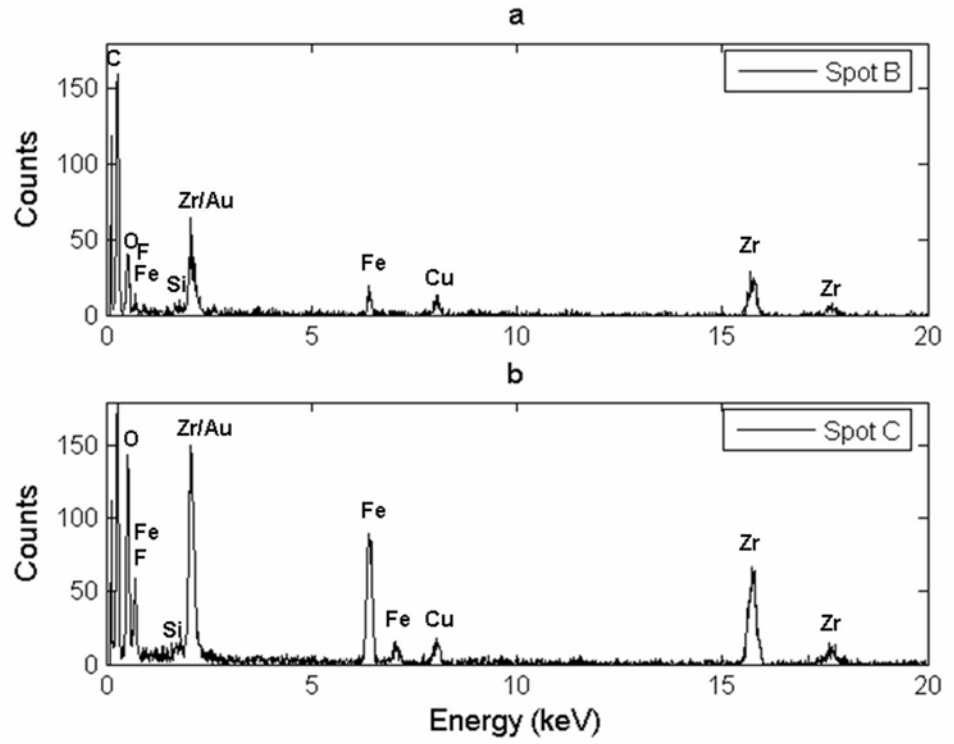

Figure 10: Spot EDS on Site B (a) and Site C (b) of the MFZ coating shown in Figure 9b.

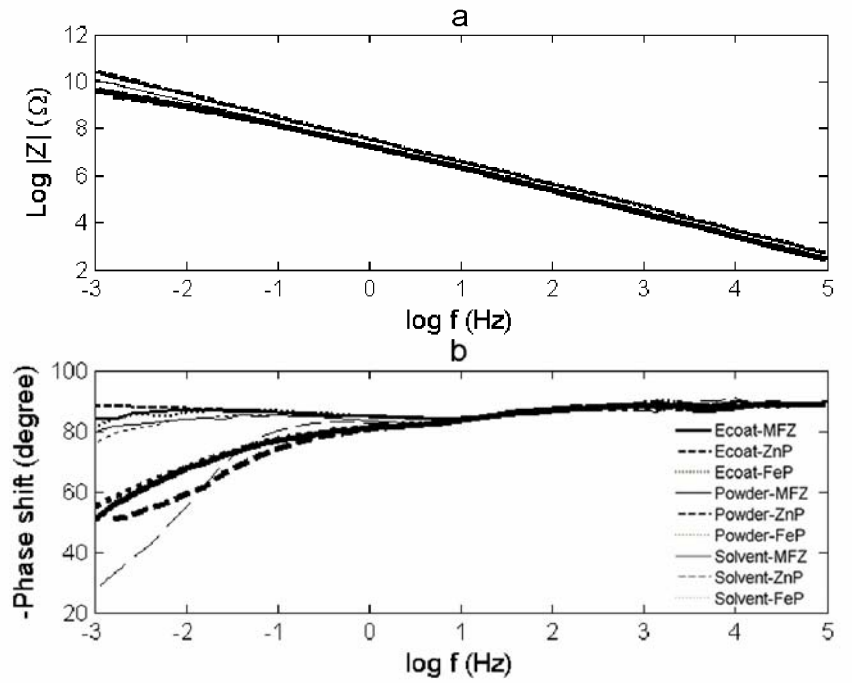

Figure 11: EIS of pretreated CRS with electrodeposited paint (Ecoat) at 70th day of immersion, with powder paint (Powder) at 70d and solvent-borne paint (Solvent) at 60d. ZnP: pretreated with zinc phosphate. FeP: pretreated with iron phosphate. (a) Magnitude Bode plot. (b) Phase Bode plot. Testing area was 28.3 cm^2.

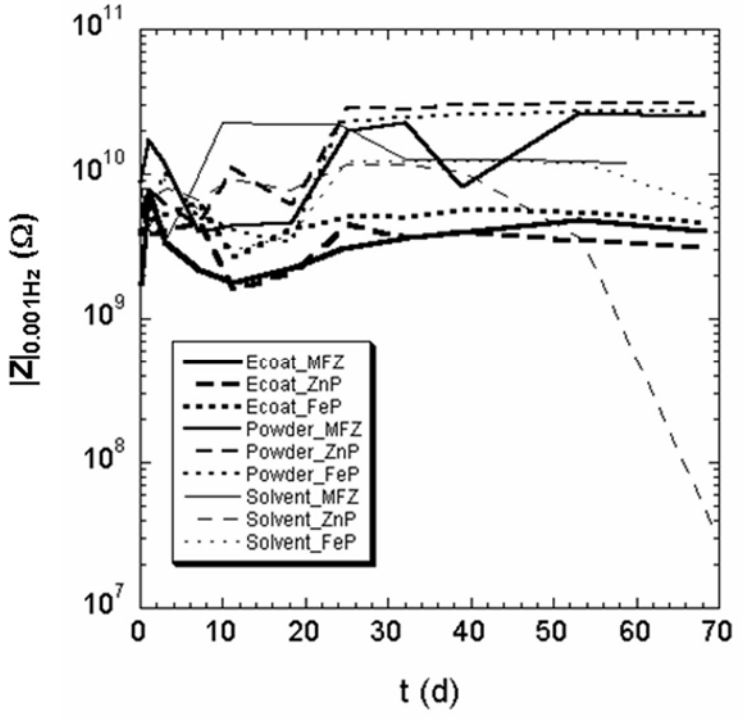

Figure 12: Evolution of |Z| at 0.001Hz for fully painted CRS with three paints and three types of pretreatment.

REFERENCES

1. **Van Wazer, J.R., ed. *Phosphorous and its Compounds*. Vol. II. 1967, Interscience Publishers Inc.: New York.**
2. **Sankara Narayanan, T.S.N., *Surface pretreatment by phosphate conversion coatings-a review.* Reviews on Advanced Materials Science, 2005. 9(2): p. 130-177.**
3. **Hirai, S., et al., *Alkaline corrosion resistance of anodized aluminum coated with zirconium oxide by a sol-gel process.* Journal of the American Ceramic Society, 1998. 81(12): p. 3087-3092.**
4. **Di Maggio, R., L. Fedrizzi, and S. Rossi, *Effect of the chemical modification of the precursor of ZrO2 films on the adhesion of organic coatings.* Journal of Adhesion Science and Technology, 2001. 15(7): p. 793-808.**
5. **Fedrizzi, L., et al., *The use of electrochemical techniques to study the corrosion behaviour of organic coatings on steel pretreated with sol-gel zirconia films.* Electrochimica Acta, 2001. 46(24-25): p. 3715-3724.**
6. **Li, H.B., et al., *Corrosion protection of mild steel by zirconia sol-gel coatings.* Journal of Materials Science Letters, 2001. 20(12): p. 1081-1083.**
7. **Gusmano, G., et al., *Zirconia primers for corrosion resistant coatings.* Surface & Coatings Technology, 2007. 201(12): p. 5822-5828.**
8. **Puomi, P., et al., *Comparison of different commercial pretreatment methods for hot-dip galvanized and Galfan coated steel.* Surface & Coatings Technology, 1999. 115(1): p. 70-78.**
9. **Puomi, P., et al., *Optimization of commercial zirconic acid based pretreatment on hot-dip galvanized and Galfan coated steel.* Surface & Coatings Technology, 1999. 115(1): p. 79-86.**
10. **Puomi, P., H.M. Fagerholm, and A. Sopanen, *Parameters affecting long-term performance of painted galvanised steels.* Anti-Corrosion Methods and Materials, 2001. 48(3): p. 160-170.**
11. **Verdier, S., et al., *Monochromatized x-ray photoelectron spectroscopy of the AM60 magnesium alloy surface after treatments in fluoride-based Ti and Zr solutions.* Surface and Interface Analysis, 2005. 37(5): p. 509-516.**
12. **Verdier, S., et al., *An electrochemical and SEM study of the mechanism of formation, morphology, and composition of titanium or zirconium fluoride-based coatings.* Surface & Coatings Technology, 2006. 200(9): p. 2955-2964.**
13. **Stromberg, C., et al., *Synthesis and characterisation of surface gradient thin conversion films on zinc coated steel.* Electrochimica Acta, 2006. 52: p. 804-815.**
14. **Campestrini, P., et al., *Investigation of the chromate conversion coating on Alclad 2024 aluminium ally: effect of the pH of the chromate bath.* Electrochimica Acta, 2002. 47: p. 1097-1113.**